classified through two pathways, i. e. direct four-electron pathway and two-electron pathway. For the first pathway, one oxygen molecule receives $4e^-$ and is reduced to $4OH^-$. For the second pathway, the oxygen molecule is firstly reduced to o $H_2O_2$ or $HO_2^-$ intermediate, then the intermediate transfers into electrolyte or is further reduced to $OH^-$ *via* receiving $2e^-$ (indirect four-electron pathway) [17]. The silver in the general case catalyzes the direct $4e^-$ reaction pathway and also the $HO_2^-$ anion disproportionation, being cheaper in comparison to conventional precious metal catalysts such as Pt, Au and Pd [18].

In our study we built the AL of the GDE using bimetallic catalysts and Teflon as a binder. For the gas diffusion layer, we applied teflonized carbon black and used a technology developed in IEES-BAS [19]. The aim of this study is to show the advantages of two of the most widely used electrocatalysts (γ-$MnO_2$ and Ag) in operation as bi-functional catalysts for ORR and OER. The obtained results were compared with the GDE with same GDL and different AL ($Co_3O_4$ and Ag). The focus of the current investigation is the influence of different catalysts on the electrochemical properties of GDE. Moreover, the varying ratio between the catalysts and their particle size is also studied.

## EXPERIMENTAL

### *Electrode preparation*

The GDL for both investigated GDEs was produced from Vulcan XC-72 R (Cabot corp., 30 nm particle size) which was modified by polytetrafluoroethylene (PTFE) (60 wt % dispersion in $H_2O$, 0.05-0.5 μm, Sigma Aldrich). The carbon blacks were teflonized up to 60 wt%. GDL was applied in a pressform completely covering its inner surface. The relative density of the layer was 50 $mg.cm^{-2}$. The AL was applied on the tightly placed GDL. It contains a bifunctional catalyst and 10 wt.% PTFE (10 μm particle size) powder (Sigma Aldrich), taken per the mass of catalysts. The bifunctional catalyst was composed, in one case of $Co_3O_4$ (Sigma Aldrich), particle size <50 nm + Ag (Ferro AG), particle size 4-30μm (30:70 wt.%) [19] and in the other case, after ratio optimization of γ-$MnO_2$ (EMD), particle size 40 μm and the same Ag (50:50 wt.%). The working area of the GDEs was 10 $cm^2$. The relative density of this layer is 40 $mg.cm^{-2}$, where the GDL was again applied by sealing the inner area of the pressform. A stainless steel mesh (Hebei Standard Filter Equipment), mesh count 100 was placed on top of the AL for the current collector. Pressure of 300 $kg.cm^{-2}$ was applied to the pressform for 3 minutes at 300˚C.

### *Experimental conditions*

The charge/discharge tests were conducted using a six-channel Galvanostat 54 (PMC) testing system. The cell discharge was controlled by limiting time or voltage. The charge is defined by time up to 45 min and voltage limit up to +2 V and time up to 30 min and voltage limit -1 V for discharge, respectively. The polarization, charge/discharge tests and impedance analysis were carried out in a specially designed three-electrode half-cell configuration in 6M KOH - electrolyte and using reversible hydrogen electrode (RHE) (Gaskatel) for reference electrode, and stainless steel mesh as a counter electrode. The impedance measurements were conducted on GAMRY Instruments Reference 3000 potentiostat/ galvanostat in a frequency range of 100 kHz to 10 mHz with ten points per decade. Sine signal of 10 mV peak to peak was applied.

## RESULTS AND DISCUSSION

### *Structure and morphology*

XRD analysis (shown on Fig. 1) reveals a mixture of Ag/$Co_3O_4$ and a small amount of fcc-alloy (or $CoC_x$) and Ag/γ-$MnO_2$ for the respective catalysts. The XRD patterns do not show formation of new phases after the electrodes were used. A strong widening of the diffraction peaks of silver was observed due to the reduction in the size of the crystallites (Table 1).

The morphology of the catalysts, as well as of the GDEs prepared with them was examined using scanning electron microscopy (SEM). On Figs. 2 and 3 the microphotographs of the studied ALs of GDE at different magnifications are shown. From the SEM images in Fig. 2 it is clear how the smaller spherical $Co_3O_4$ particles cover the larger silver particles. At higher magnification (×3000 and × 10000) a layered structure is clearly observed. In Fig. 3, in the AL prepared from a mixture of Ag/γ-$MnO_2$, rough morphology and homogeneous particle distribution of the two catalysts are observed. Additionally, the smaller irregularly shaped silver particles, which are in a fairly wide range, almost completely envelop the larger particles of γ-$MnO_2$. The microphotographs of the different GDEs show significant differences in the particles' morphology and size as well.

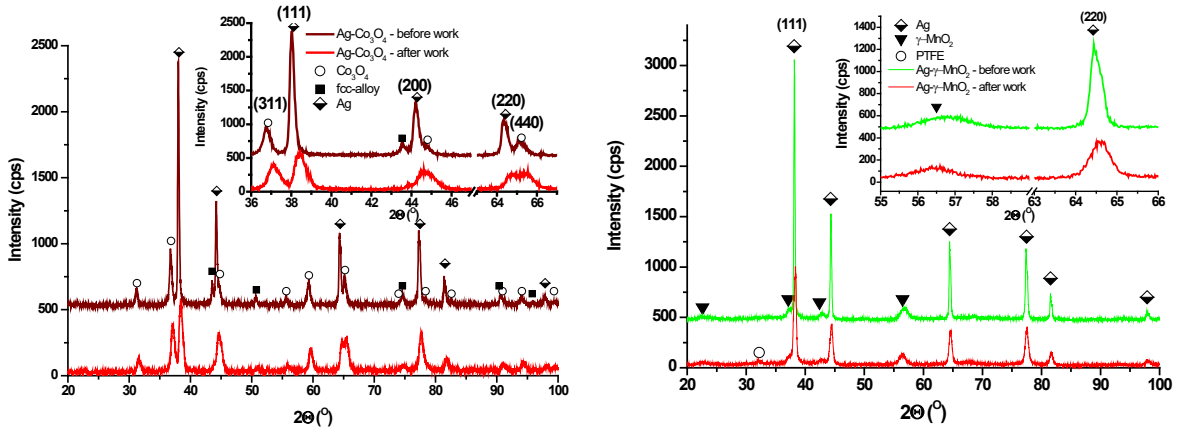


**Fig. 1.** XRD phase analysis of the prepared electrodes with bimetallic structure ($Ag/Co_3O_4$ and $Ag/\gamma\text{-}MnO_2$) before and after work

**Table. 1.** XRD parameters of GDEs with different AL

| | Phases | Average crystalline size, nm | |
|---|---|---|---|
| | | Ag | $Co_3O_4$ or $MnO_2$ |
| Ag-$Co_3O_4$-before work | Ag+$Co_3O_4$, fcc-alloy | 49 | 18 |
| Ag-$Co_3O_4$-after work | Ag+$Co_3O_4$, fcc-alloy | 15 | 13 |
| $MnO_2$-Ag-before work | Ag+γ-$MnO_2$ | 50 | 8 |
| $MnO_2$-Ag-after work | Ag+γ-$MnO_2$ PTFE | 18 | 8 |

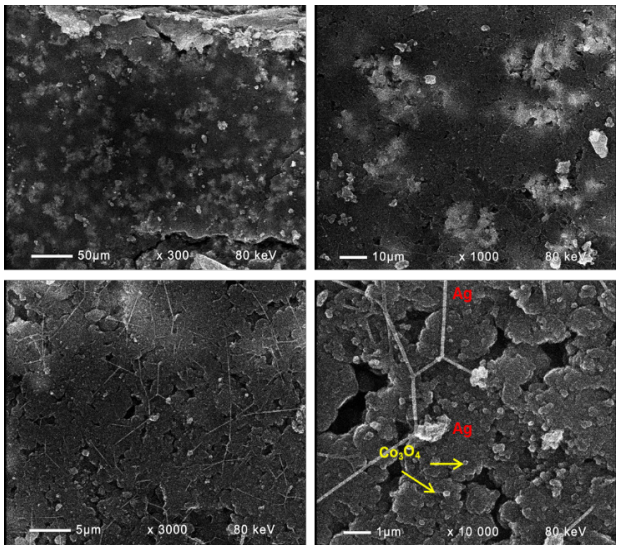


**Fig. 2.** SEM micrographs of GDE with bimetallic AL ($Ag/Co_3O_4$)

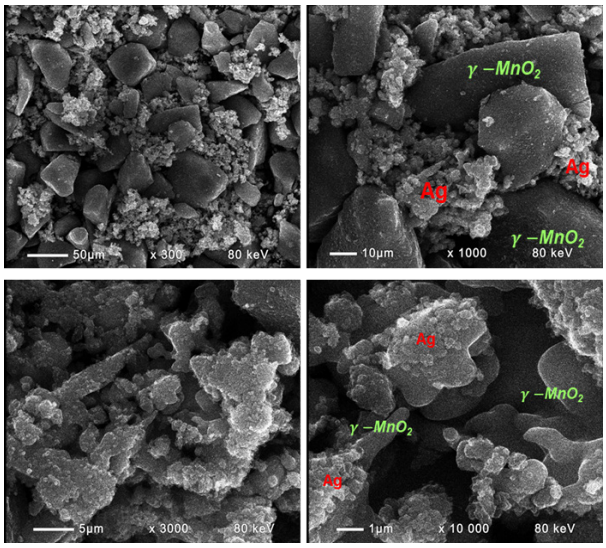


**Fig. 3.** SEM micrographs of GDE with bimetallic AL ($Ag/\gamma\text{-}MnO_2$)

*BET analysis*

A study by BET analysis revealed a high specific surface area of the gas diffusion layer (GDL) in GDEs with bi-metallic catalysts in the AL. The average size of the mesopores is about 10.7 nm which is a prerequisite for the predominance of Knudsen diffusion. The presence of this type of diffusion is also a prerequisite for the fastest and most efficient access of oxygen to the catalytic surface and is the reason for the high values of diffusion-limited current density $i_d$ (for ORR).The undergoing of this type of diffusion is also one of the explanations for the good discharge characteristics of these GDEs. Moreover, the BET analysis has given another important information that the GDL has a high specific surface area of 118.8 $m^2.g^{-1}$ and total pore volume (for pores smaller than 132 nm) of 0.318 $cm^3.g^{-1}$, which is probably another reason for the facilitated access of oxygen to the AL.

*Electrochemical characterization*

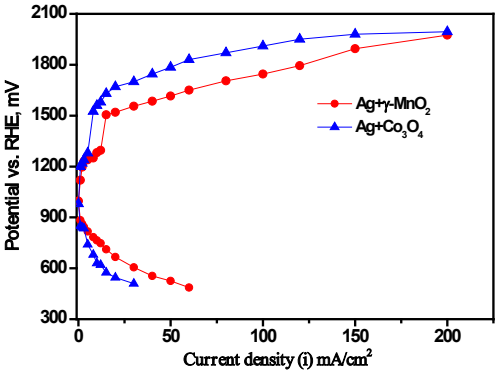


**Fig. 4.** Polarization curve of GDEs with different CL

On Fig. 4 the volt-ampere characteristics of the investigated GDEs are shown. It can be clearly seen that the use of the mixture Ag/$Co_3O_4$ for the obtaining of the AL in the GDE current density of 30 mA.cm$^{-2}$ was achieved for the ORR. With replacement of the $Co_3O_4$ with γ - $MnO_2$ the applied current density for the electrochemical discharge considerably increases – up to 60 mA.cm$^{-2}$. Moreover, the GDE efficiency standard for OER is potential-$E_{10}$ [20]. For the investigated GDEs the values were $E_{10}$=1295 mV for Ag/$Co_3O_4$ AL and $E_{10}$= 1282 mV for Ag/γ-$MnO_2$, which additionally confirmed the good electrochemical behavior of the two investigated GDEs. With the use of the two mixtures of bi-metallic catalysts a leap is observed in the interval of 1200-1550 mV in the polarization curves of the silver containing electrode. That effect was carefully studied by Amin [21] and is related to the formation of $Ag_2O$ and/or $Ag^{I}Ag^{III}O_2$ during the OER. Long-term tests of the two GDEs showed very good mechanical stability of over 300-500 charge/ discharge cycles (Fig. 5a) and b)). That is also confirmed by the very smooth increase (almost insignificant) of polarization between the first and last cycle at GDE with Ag/γ-$MnO_2$ structure (Fig. 5 b).

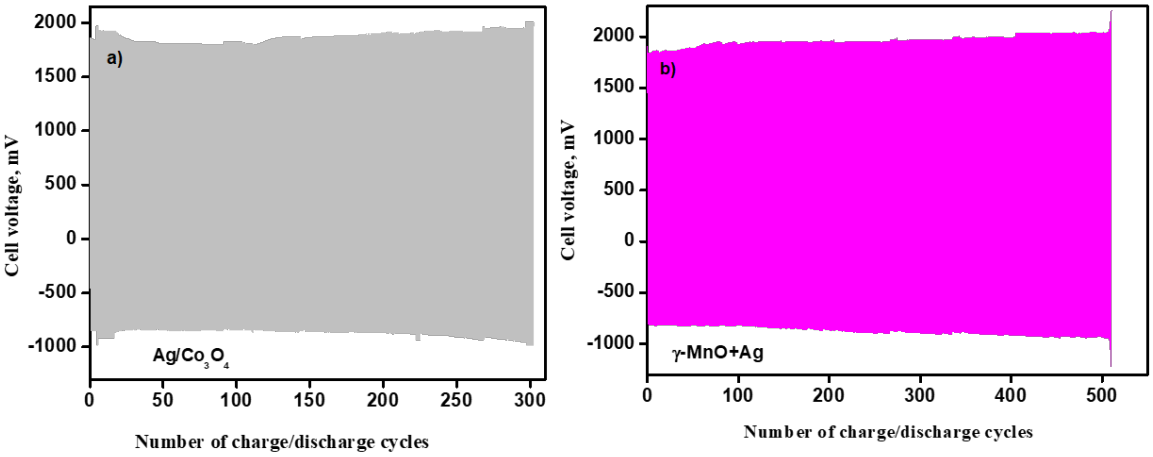


**Fig. 5.** Durability test of the GDEs with a) Ag/$Co_3O_4$ and b) Ag/γ-$MnO_2$

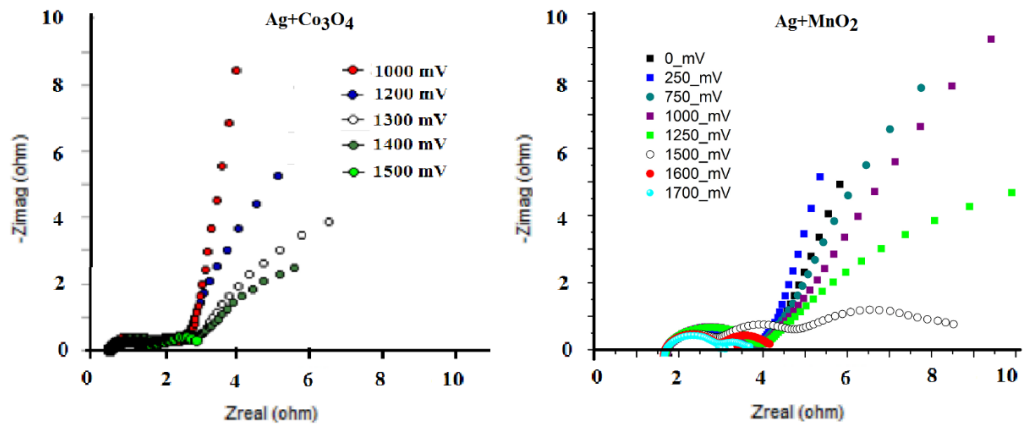


**Fig. 6.** Nyquist plots of impedance spectra of the GDEs with Ag/$Co_3O_4$ and Ag/γ-$MnO_2$.

### *EIS investigations*

Fig. 6 shows the Nyquist plots of the Ag/$Co_3O_4$ and Ag/γ - $MnO_2$ electrodes at different potentials. From high to medium frequencies, the impedance spectra consist of partially overlapping semicircles and remain almost unchanged with increasing potential mainly due to the heterogeneous structure of the electrodes (the resistance of the pores, particles and boundaries between them) without a contribution by the electrochemical processes. Conversely, the impedance at low frequencies depends on the applied potential and reflects the electrochemical behavior of the electrodes. At lower potentials, far from the OER potential, the electrode behaves as a pseudocapacitor (slanted line) due to the formation of an electric double layer. As the potential increases, the line at low frequencies gradually bends and a new depressed semicircle with decreasing diameter is formed in a result of the OER with a decreasing charge transfer resistance (Rct). At the higher potentials (over 1500 mV) Rct becomes very small and the semicircle is not distinguished.

## CONCLUSIONS

GDEs with different AL (Ag/$Co_3O_4$ and Ag/γ-$MnO_2$) and same GDL were investigated with modern physical and electrochemical methods. From these studies, it was found out that the equable weight distribution of the two catalysts (1:1) with Ag/γ-$MnO_2$ and their almost equal particle sizes give good results (higher than those with cobalt and silver) in the operation of the secondary GDE. Statistically, this morphology also determines a homogenous distribution of the pores (observed in the SEM microphotograph), from which it follows that the active sites for the two oxygen reactions are almost equally distributed in the volume of the catalytic layer. The EIS analysis gives the impression that the electrochemical behavior of the investigated GDEs also shows a behavior similar to that of supercapacitors. In future studies, more thorough attention will be paid to this fact.

***Acknowledgements:*** *The authors kindly acknowledge the financial support of project № BG05M2OP001-1.002-0014 „Center of Competence HITMOBIL - Technologies and Systems for Generation, Storage and Consumption of Clean Energy", funded by Operational Programme "Science and Education for Smart Growth" 2014-2020, co-funded by the EU from European Regional Development Fund. This work is partially supported by the Bulgarian Ministry of Education and Science under National Roadmap for Scientific Infrastructure (CMD No. 354 of 29.06.2017) "Distributed infrastructure of centers for synthesis and characterization of new materials and conservation of archeological and ethnographic artefacts, INFRAMAT" (Contract D01-306/20.12.2021).*

## REFERENCES

1. B. Abrashev, M. Slavova, E. Mladenova, V. Terziev, B. Burdin, G. Raikova, K. Petrov, *Journal of Chemical Technology and Metallurgy*, **56** (6), 1261 (2021).
2. C. Wang, Y. Yu, J. Niu, Y. Liu, D. Bridges, X. Liu, J. Pooran, Y. Zhang and A. Hu, *Applied Sciences*, **9** (14), 2787 (2019).
3. J. Yi, P. Liang, X. Liu, K. Wu, Y. Liu, Y. Wang, Y. Xia, J. Zhang, *Energy Environ. Sci*., **11**, 3075 (2018).
4. L. Yaqoob, T. Noor, N. Iqbal, *Journal of Energy Storage,* **56**, 106075 (2022).
5. M. Karwowska, T. Jaron, K. J. Fijalkowski, P. J. Leszczynski, Z. Rogulski, A. Czerwinski, *J. Power Sources*, **263,** 304 (2014).
6. Y. J. Wang, B. Fang, D. Zhang, A. Li, D. P. Wilkinson, A. Ignaszak, L. Zhang, J. Zhang, *Electrochem. Energy Reviews*, **1**, 1 (2018).
7. A. G. Olabi, E. T. Sayed, T. Wilberforce, A. Jamal, A. H. Alami, K. Elsaid, S. M. A. Rahman, S. K. Shah, M. A. A., *Energies*, **14**, 7373 (2021).
8. H. Aldave, E. Andreoli, *Catalysts*, **10**, 713 (2020).
9. R. Ponnusamya, R. Venkatesanb, M. Kandasamyc, B. Chakrabortyd, C. S. Routa, *App. Surface Science*, **487**, 1033 (2019).
10. J. Zhang, Q. Zhou, Y. Tang, L. Zhang, Y. Li, *Chem. Sci*., **10**, 8924 (2019).
11. H. Radinger, P. Connor, R. Stark, W. Jaegermann, B. Kaiser, *Chem. Cat. Chem.*, **13**, 1175 (2021).
12. S. Dey, V. V. P. Kumar, *Current Research in Green and Sustainable Chemistry,* **3**, 100012 (2020).
13. D. Pletcher, X. Li, S. W. T. Price, A. E. Russell, T. Sönmez, S. J. Thompson, *Electrochim. Acta*, **188**, 286 (2016).
14. J. Shin, J. K. Seo, R. Yaylian, A. Huang, Y. S. Meng, *International Materials Reviews*, **65**, 6 (2020).
15. X. He, F. Yin, G. Li, *Int. J. Hydrog. Energy*, **40**, 9713 (2015).
16. H. Osgood, S. V. Devaguptapu, H. Xu, J. Cho, G. Wu, *Nano Today*, **11,** 601 (2016).
17. Q. Liu, Z. Pan, E. Wang, L. An, G. Sun, *Energy Storage Materials*, **27**, 478 (2020).
18. F. W. T. Goh, Z. Liu, X. Ge, Y. Zong, G. Du, T. S. A. Hor, *Electrochim. Acta*, **114**, 598 (2013).
19. B. Abrashev, D. Uzun, A. Kube, N. Wagner, K.Petrov, *Bulg. Chem. Comm*., **52** (2), 245 (2020).
20. M. Tahira, L. Pana, F. Idreesd, X. Zhanga, L. Wanga, J. J. Zoua, Z. L. Wangb, *Nano Energy*, **37**, 136 (2017).
21. H. M. A. Amin, H. Baltruschat, D. Wittmaier, K. A. Friedrich, *Electrochim. Acta*, **151**, 332 (2015).